P-044

An integrated inversion of seismic refraction and reflection data using combined wave-equation tomography and full waveform inversion

Haiyang Wang, Satish C. Singh, IPGP, France, and Henri Calandra, TOTAL, France*

Summary

We have developed an integrated method to obtain high- resolution subsurface elastic parameters using combined wave equation tomography (WET) and full waveform inversion (FWI). Both refraction and reflection data are used. During parameterization, long wavelength and short wavelength structures are separated and mapped into velocity and density to account for kinematics and dynamics, respectively. Full wavefield modeling is used to compute synthetic data that include all reflection and refraction arrivals. To better constrain the reflection amplitude, the near offset data are first inverted using FWI where all the model perturbations are mapped into density. The short wavelength density structure is then converted into vertical travel time domain where it is independent of long wavelength velocity model. The WET is applied to both reflection and refraction data. As long wavelength structure (velocity) is updated, short wavelength structure is converted back into depth domain for wavefield computation. Finally FWI is applied all the data to retrieve short wavelength structures with resolution up to a quarter wavelength. The method is applied to two synthetic examples; our results shows that one can recover detailed velocity information starting from a model far from the final model.

Keywords: *Wave-equation, tomography, reflection, refraction, FWI*

Introduction

As the emergence of high performance computing, FWI is becoming an important tool to determine the subsurface physical properties at fine scale (Tarantola, 1984; Mora, 1987; Pratt et al., 1998), but nonlinearity present in waveform inversion still poses serious problem. The nonlinearity of FWI can be alleviated by providing a good starting model that contains correct kinematic information and place synthetic seismic arrivals within a half-period to real data. Even with a good starting model, multi-scale strategy, either starting with very low frequency or with long offset data, is required (Bunks et al., 1995; Shipp and Singh, 2002; Sirgue and Pratt, 2004). Wave-equation tomography applied to first arrivals (Luo and Schuster, 1991; Wang et al., 2012) can provide a good starting point and regularization for FWI as it shares the same inversion mode as FWI. However, in surface seismic survey, the WET requires very long offsets to record refraction waves propagating in the deep part of the model. Furthermore, in the presence of high velocity near surface layers, WET using refraction waves can hardly resolve any structure beneath this layer due to the lack of deep information. So we need to incorporate reflection arrivals into WET to provide more constraints.

The use of reflection wave in the FWI mode to retrieve long wavelength structure has been proposed to reduce the nonlinearity of FWI (Clement et al., 2001; Plessix et al., 1999; Xu et al., 2012). Model parameters need to be separated into long and short wavelengths that account for kinematics (phase) and dynamics (amplitude), respectively, while short wavelength structure is dependent on long wavelength structure. In this study, we propose to use velocity and density, which provide a convenient way for wavefield modeling. Migration operators are usually used to generate short wavelength structure, i.e., reflectivity or impedance. Here we use near offset FWI to map the impedance contrast into density. The inverted short wavelength density model and long wavelength velocity model is used to produce

1 Rue Jussieu, 75005, Paris, France
Email: singh@ipgp. fr,

synthetic data that includes including both refraction and reflection waves. For WET, misfit is the cross-correlation of waveform delay between synthetic and real data. Taking advantage of the vertical travel time invariant property of zero-offset short wavelength structure (Snieder et al., 1989; Plessix, 2012), we can convert density from depth domain into time domain at the preliminary stage. As velocity is updated using WET, we can convert density back to depth domain to perform modeling for next iteration.

We combine refraction and reflection for WET and demonstrate the applicability of the method on two synthetic examples. The results show the advantage of using combined data over using only refraction, which turns out to be critical for later stage for the FWI to converge to the global minimum.

Integrated inversion using WET and FWI

Following the approach by Wang et al. (2012), we use a hybrid misfit function to jointly use WET and FWI, which allows us to invert for high-resolution subsurface structure starting from poor long wavelength velocity model:

$$H = \alpha H_t + (1-\alpha) H_{FWI}. \qquad (1)$$

H_{FWI} is the classic least-square FWI misfit function and H_t is cross-correlation time delay misfit for WET. At the early stages of inversion, we can set α equal to 1, which means we just perform WET. Then after misfit is reduced to a certain threshold for WET, FWI can be switched on with the regularization of Ht. Gradient regularization and preconditioning as shown in Wang et al. (2012) is also adapted here to accelerate the convergence.

WET for refraction and reflection waves

WET aims to minimize L2 norm cross-correlation delay between synthetic and real data (Luo and Schuster, 1991),

$$H_t = \frac{1}{2}\sum_s\sum_r(\Delta\tau_1^2/\sigma_{\Delta\tau_1}^2 + \Delta\tau_2^2/\sigma_{\Delta\tau_2}^2), \qquad (2)$$

where $\Delta\tau_1$ and $\Delta\tau_2$ are the waveform delay for refraction and reflection data, respectively, which maximizes the cross-correlation function:

$$CC_{\max}(\Delta\tau) = \int d_{real}(t+\Delta\tau) d_{syn}(t)\,dt\,. \qquad (3)$$

A window should be selected prior to cross-correlation. We use a semi-automatic global picking method to extract coherent phases. $\sigma_{\Delta\tau_1}$ and $\sigma_{\Delta\tau_1}$ are the covariance for refraction and reflection delay measures, which are used to normalize the refraction and reflection misfit measures, and hence they equally weight their contributions.

In WET, the gradient of H_t with respect to model parameter p can be expressed as (Tromp et al., 2005):

$$g_t = \sum_s\int_V[\sum_r \Delta\tau K_p \delta p]dV\,. \qquad (4)$$

K_p is its sensitivity kernel for a certain phase and generally is of "banana-donuts" shape. Gradient g_t is actually the sum of the weighted kernels by waveform delays for all source- receiver pairs. Compared to single ray path for conventional ray based tomography, WET extends the sensitivity area to Fresnel volumes and hence provides extra "off-raypath" information. The kernel is calculated by back-propagating the synthetic waveform in reverse time sense at receiver positions and cross-correlating it with forward propagating wavefield from source position.

$$K_p = \int_0^T G(x,x_s;t) * G(x,x_r;T-t)\,dt. \qquad (5)$$

G is Green's function. Once gradient g_t is calculated, we can use local search methods, such as steepest descent or conjugate gradient method to update model parameters iteratively.

Model scale separation by parameterization

In this paper we use a finite difference elastic wave equation operator **F** to calculate G, i.e., synthetic data $\mathbf{d}_{\text{syn}}$,

$$\mathbf{d}_{syn} = \mathbf{F}(M, \Delta M, s), \qquad (6)$$

in which, M and ΔM represent the long and short wavelength structures, respectively. s is the source wavelet. Since our objective is to retrieve the kinematic information for FWI, we propose to use velocity V as long wavelength model component. Short wavelength structure is needed to generate reflection waves for comparison with real data. It contains dynamic information and holds almost linear relationship with waveform amplitude. It can be mapped to reflectivity

(Plessix, 1999; Xu et al., 2012) in migrationbased traveltime tomography mode or impedance in the scope of classic FWI (Tarantola, 1986; Snieder et al., 1989). It is also dependent on the long wavelength structure. As we keep velocity update ΔV to be long wavelength component, we can separate the short wavelength component by mapping it to density $\rho(V)$, which means density will contain all the variation in impedance. Then Eq. (6) can be recast as:

$$\mathbf{d}_{syn} = \mathbf{F}(V_0 + \Delta V, \rho_0(V) + \Delta\rho(V), s)\,. \qquad (7)$$

Long wavelength ΔV is estimated using WET and the short wavelength $\Delta\rho(V)$ is obtained using FWI operator $\mathbf{F}^*_{FWI}$, which can be regarded as the adjoint of $\mathbf{F}$.

$$\Delta\rho(V) = \mathbf{F}^*_{FWI}(V, \rho_0(V), \mathbf{d}_{real}), \qquad (8)$$

In WET we extract the phase delay information by normalized cross-correlation, which is insensitive to AVO variation as long as phases are identical in synthetic and real data. As a result, we just use the near-offset data to invert for density contrast to save computation time. Furthermore, we can convert $\Delta\rho$ from depth to zero-offset vertical travel time domain by a simple coordinate transformation (Snieder et al., 1989; Plessix, 2012):

$$\tau(z) = \int_0^z \frac{dz'}{V(z')}, \qquad (9)$$

or vice versa through the adjoint of Eq.(9):

$$z = \int_0^\tau V(\tau')d\tau'(z)\,. \qquad (10)$$

Notice that $\Delta\rho(\tau)$ is invariant to velocity change and we have stationary reflections at zero offset. During WET iterations, $\Delta\rho(\tau)$ is converted back to depth domain using Eq.(10) for modeling in Eq.(6). $\Delta\rho(V)$ will be shifted, compressed and stretched as inversion iterates. The advantage of the coordinate transformation is that we only need to perform Eq.(8) very few times during the inversion instead of one time for each iteration.

Summary of practical workflow

Given the large model space and nonlinearity of seismic waveform inversion problem, we propose the following steps to save computation time and guide the inversion to converge to global minimum effectively.

1. Starting from poor initial model V_0, run WET using only refraction wave to provide a good estimation of V_1.
2. Run FWI using only near-offset reflection data to update short wavelength $\Delta\rho(V_1)$ and convert it to $\Delta\rho(\tau)$ using Eq.(9).
3. Use Eq. (7) to model synthetic data and run WET using combined refraction and reflection waves to get long wavelength velocity update ΔV. In each iteration of WET, $\Delta\rho(\tau)$ is converted to $\Delta\rho(V_1 + \Delta V)$ as input for Eq. (7).
4. For substantial update ΔV, run step 2 again and repeat step 3.
5. Initialize FWI using whole waveform once H_t reaches our conversion criteria.

Application to 1-D blocky model

To demonstrate the different aspect of our method, we apply our strategy to a simple 4-layer blocky model (Fig.1) with sharp velocity contrasts. We use 7.5 Hz central frequency Ricker wavelet as source and maximum 8 km offset data. Initial model is a gradient model with velocity increasing slowly with depth (Fig.1), which contains minimum information of the real model, and is far from the true model.

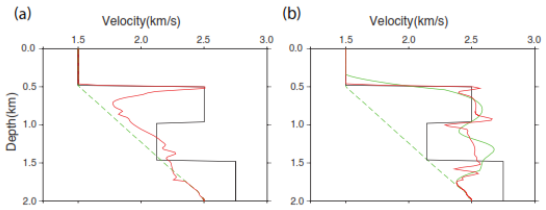

Figure 1: 1D synthetic test. Left: Result after FWI using gradient model as starting model. Right: Result after "refraction WET + FWI" approach. True velocity (solid black line), linear gradient velocity (dashed green line), model after refraction WET (solid green line) and FWI velocity after 100 iterations (solid red line).

Since we have reasonable low frequency and long offset data, we first perform multi-scale FWI following Shipp and Singh (2002). Due to the poor starting model and high velocity contrasts, FWI fails to converge to the global minimum after 100 iterations (Fig.1), and provides wrong solution.

In the next step, we performed "refraction WET + FWI" approach of Wang et al. (2012). Original data is shown in Fig.(2). We can observe that due to the high velocity in the second layer and limited offset, no refractions from the last layer are present. So we can expect no reliable model update below the second

layer if we use only refraction waves. After 25 iterations of WET, we recover the velocity of the second layer very well but almost no information on deep layers other than regularization effect (Fig.1). The FWI fails again to retrieve the long wavelength update in the deep part of the model because the kinematics in incorrect, but it does provide information about the interfaces.

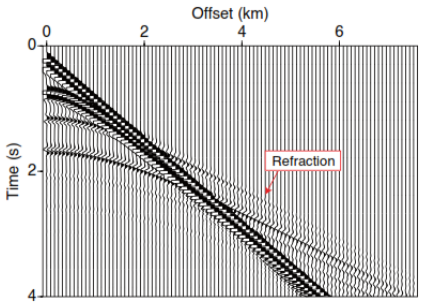

Figure 2: Modeled data using true model. Three reflection and refraction waves are used for WET.

Figures (3) and (4) show the results of our integrated approach. Starting from WET results using only refraction waves, we perform near-offset FWI for 25 iterations and obtain the density model shown in Fig. (3). Since we have a good constraint for the second layer, the second reflector is located almost at the correct depth. The third reflector, however, is pushed down due to the wrong high velocity there. Note that since we map all the impedance contrast to density, the density contrast is slightly higher than the true impedance contrast. Then we combine refraction and

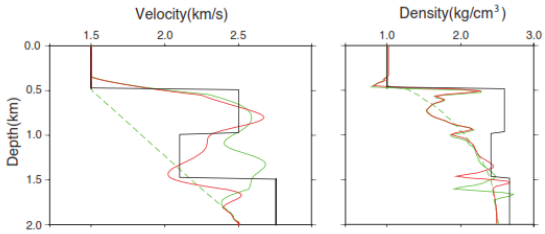

Figure 3: Velocity and density results of combined refraction/reflection WET. True modes (black solid line), starting models (dashed green line), models after refraction WET in step1 (solid green line) and models after combined refraction & reflection WET (solid red line).

reflection waves for WET. After 25 iterations, we reduce 97% time delay residual. The final average misfit is 14 ms, which is less than one quarter of dominant period. FWI is then initialized and after 50 iterations the final model fits the true model well with a normalized residual reduction of 95%. Note that we have no resolution of the final layer so we can only retrieve the velocity contrast. In order to constrain the last layer, we would require either longer offsets or another reflector below this layer.

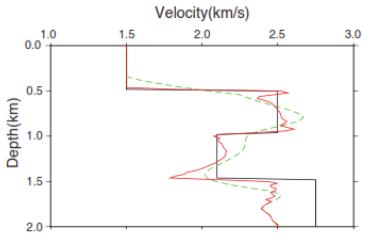

Figure 4: Final velocity model after 50 iterations of FWI.

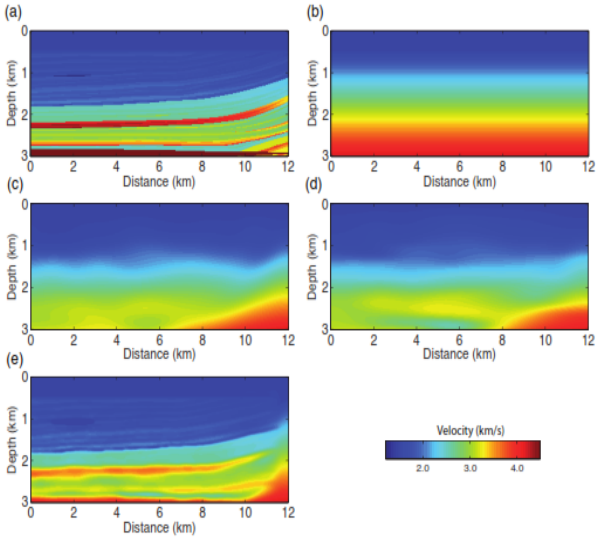

Figure 5: 2-D test results. (a) True model. (b) Starting model. (c) Refraction WET result. (d) Combined refraction/reflection WET result. (e) FWI result using (d) as starting model.

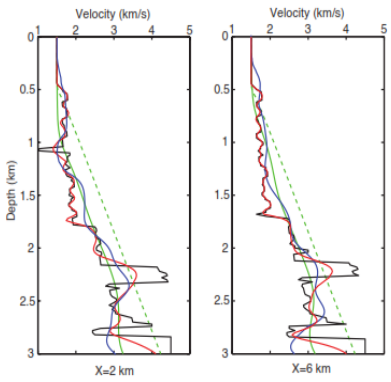

Figure 6: Velocity logs from Fig.(5). True velocity model (blackline), starting model (green dashed line), Refraction WET model (solid green line), combined refraction/reflection WET result (blue line), FWI model (red line).

Application to 2-D model

To further show the robustness of our strategy, we apply it to a 2-D model (Fig.5a), which is part of a modified version of Marmousi-2 model. The target area is 12 km long and 3 km deep. Ricker wavelet with central frequency 7.5 Hz is used as the source. 56 shots with a spacing of 200 m range from 0.5 km to 11.5 km within the model. A 10 km long streamer with 500 receivers is used for acquisition at 15 m below the sea surface. In the test, model is extended by 10 km to the left to accommodate for the acquisition geometry. Starting model is a 1-D gradient model that is faster than true model (Fig.5b).

Three steps of inversion are the same as for the 1-D test. Fig.(5c) and Fig.(5d) show the WET results using refraction (first step) and combined refraction/reflection (second step) after 25 iterations, respectively. Fig.(5e) shows the final result after 25 iterations of FWI. Average time delay decrease from about 400 ms to 25 ms. Waveform residual reduction is ~ 96%. 1-D velocity logs at distance 2 km and 6 km are shown in Fig.(6).

WET result using refraction provides the smoothed long- wavelength component of the true model (Fig.5c). But the sharp velocity contrasts can be hardly observed. Then WET using combined refraction/reflection successfully retrieves more features of the true model, including better-confined layering, gas saturation and deep velocity variations (Fig.5d, Fig.6). Starting from this model, FWI can converge fast to global minimum (Fig.5e). Due to the relatively low frequency, we can only recover limited sharp velocity contrast. To further improve the model, we need to include higher frequency data.

Discussion and conclusions

We combine refraction and reflection wave for WET to obtain robust subsurface velocity estimation, which provides correct kinematics and serves as a good starting point for FWI to converge to global minimum. Long wavelength and short wavelength scales of the model are serves as a tool to extract short wavelength density contrast, which is converted to vertical travel time domain and depth domain back and forth during WET. Since we reject the amplitude effect by normalized cross-correlation in WET, our strategy is robust to cycle skipping problem than classical least-square FWI mode.

Acknowledgements

The authors would like to thank TOTAL for the financial support and the permission to publish this work. The authors also thank Francois Auderbert and René-Edouard Plessix (Shell) for discussion

References

Clément, F., Chavent, G. and Gomez, S., 2001, Migration- based traveltime inversion of 2-D simple structures: a synthetic example: Geophysics, 66(**3**), 845–860.

Luo, Y. and Schuster, G.T., 1991, Wave-equation traveltime inversion: Geophysics, 56(**5**), 645–653.

Min, D.J. and Shin, C., 2006, Refraction tomography using a waveform inversion back propagation technique: Geophysics, 71(**3**), R21-R30.

Mora, P., 1987, Nonlinear two-dimensional elastic inversion of multioffset seismic data: Geophysics, 52(**9**), 1211–1228.

Plessix, R.É., Y. H. De Roeck, and G. Chavent, 1999, Waveform inversion of reflection seismic data for kinematic parameters by local optimization: SIAM Journal on Scientific Computing, 20(**3**), 1033–1052.

Plessix, R.É., 2012, A pseudo-time formulation for acoustic full waveform inversion: Geophysical Journal International, 192(**2**), 613-630.

Pratt, G., Shin, C. and Hicks, 1998, Gauss-newton and full newton methods in frequency space seismic waveform inversion: Geophysical Journal International, 133(**2**), 341–362.

Shipp, R.M. and Singh, S.C., 2002, Two-dimensional full wavefield inversion of wide-aperture marine seismic streamer data: Geophysical Journal International, 151(**2**), 325–344.

Snieder, R., Xie, M., Pica, A. and Tarantola, A., 1998, Retrieving both the impedance contrast and background velocity: A global strategy for the seismic reflection problem: Geophysics, 54(**8**), 991-1000.

Sirgue, L. and Pratt, R.G., 2004, Efficient waveform inversion and imaging: A strategy for selecting temporal frequencies: Geophysics, 69(**1**), 231–248.

Tarantola, A., 1984, Inversion of seismic reflection data in the acoustic approximation: Geophysics, 49(**8**), 1259–1266.

Tarantola, A., 1986, A strategy for nonlinear elastic inversion of seismic reflection data: Geophysics, 51(**10**),1893-1903.

Tromp, J., Tape, C. and Liu, Q., 2005, Seismic tomography, adjoint methods, time reversal and banana- doughnut kernels: Geophysical Journal International,160(**1**), 195–216.

Xu, S., Wang, D., Chen, F., Lambaré, G. and Zhang, Y., 2012, Full waveform inversion for reflected seismic data: 74th EAGE Conference & Exhibition incorporating SPE EUROPEC 2012, Expanded Abstract, W024.

Wang, H., Singh, S.C., Jian, H. and Calandra, H., 2012, Integrated inversion of subsurface velocity structures using wave equation tomography and full waveform inversion: 82nd Annual International Meeting, SEG, Expanded Abstract.